Antineutrino astronomy and geophysics

Lawrence M. Krauss*, Sheldon L. Glashow† & David N. Schramm‡

* Lyman Laboratory of Physics, Harvard University, Cambridge, Massachusetts 02138, USA
† Department of Physics, Boston University, Boston, Massachusetts 02215, USA
‡ Department of Physics and Astrophysics, Enrico Fermi Institute, University of Chicago, Chicago, Illinois 60637, USA

Radioactive decays inside the Earth produce antineutrinos that may be detectable at the surface. Their flux and spectrum contain important geophysical information. New detectors need to be developed, discriminating between sources of antineutrinos, including the cosmic-background. The latter can be related to the frequency of supernovas.

IF there are more things in heaven and Earth than are dreamt of in our natural philosophy, it is partly because electromagnetic detection alone is inadequate. For sources which are visually obscured or which emit most of their energy in a form other than photons, new methods of detection must be developed. This has spurred the growth of neutrino astronomy, typified by the detection of neutrinos emitted in the interior of the Sun[1,2] but although the usefulness of the weak interactions in probing astrophysical sources has been recognized, the potential of antineutrino detection has not been widely explored. That is our objective.

We demonstrate that the Earth is a rich source of antineutrinos whose detection can provide otherwise inaccessible key information on the internal structure and dynamics of the Earth. Moreover, by a consideration of the antineutrino background from other sources, we find that there may be a diffuse background of ~10-MeV antineutrinos from supernovae which, if detected, could yield information on the energy and frequency of supernovae.

That the Earth is a source of antineutrinos was first pointed out by Eders[3] and Marx and co-workers[4–6]. Marx in particular was the first seriously to investigate the detection of terrestrial neutrinos and to recognize the importance of both resonant capture and inverse β decay of terrestrial antineutrinos in detection[4]. But a detailed analysis of the geophysical implications of the problems of measuring the actual flux of terrestrial antineutrinos has not been performed.

Earth as a source

Antineutrinos ($\bar{\nu}$) are produced in radioactive β decays of abundant isotopes inside the Earth as in

$$[A, Z] \rightarrow [A, Z+1] + e^- + \bar{\nu} \qquad (1)$$

where A, Z are the atomic number and charge of the nucleus and e^- represents the β particle (electron). Isotopes which first decay by α emission yield neutron-rich products which subsequently undergo β decay. The discovery of these processes, fundamental in the study of geophysics, drastically altered estimates of the lifetime of the Earth based on the assumption that there is no substantial production of heat within the Earth[7]. Indeed, the energy released in these decays also to a large extent determines the dynamics of its interior.

The abundance of radioactive isotopes inside the Earth is thus of prime geophysical importance, but direct sampling is possible only at or near the surface[8]. Measurements of total heat flow out of the Earth, moreover, are uncertain because of the size of local variations and the inaccessibility of much of the Earth's surface[8]. But even if present estimates of the global heat flux, centring on the value 40 TW[8–10], were much more accurate, the question of how much of the heat loss arises from production and how much from the fact that the Earth is still hot would remain unresolved. The difficulty is that heating from radioactive sources known in the surface layers is of the same order of magnitude as the total heat flux, so that even small abundances elsewhere would imply that the interior of the Earth is heating, not cooling.

Table 1 gives data for the lithosphere, which we define as the surface layer down to ~100 km depth containing the continental and sub-oceanic plates whose mass of $\sim 2 \times 10^{25}$ comprises about 1/300 of the Earth's total mass[9]. The mean abundances are given in Table 1 for the chief radioactive isotopes ^{40}K, ^{238}U, ^{232}Th, ^{87}Rb (ref. 11); actual abundances depend crucially on rock type and region[8], generally decreasing from granite to basalts to dunites, with ^{238}U and ^{232}Th abundanees varying by factors of 5–10. The abundance of ^{40}K is particularly sensitive to rock type and drops to almost zero in dunites[8].

Our first objective is to calculate the spectrum of the antineutrino flux from the Earth, using the lithospheric abundances of radioactive materials as a starting point but within the constraints of what is known of the total heat flux. In reality, heat flux and the distribution of radioactive materials are not uniform over the surface of the Earth. Both are probably enhanced in continental crust[12] while heat flow from the oceans is probably largely due to plate formation there[13]. To begin with, though, we ignore this asymmetry.

Table 1 shows that the lithospheric ^{238}U and ^{232}Th decay chains account for an average heat production of ~17 TW, far exceeding that from ^{40}K and ^{87}Rb. Total radiogenic heat production at ~19 TW is approximately half the total heat flux at the surface.

In what follows, we calculate antineutrino fluxes from lithospheric radioactive isotopes only. For while most geophysical models[13] suggest that concentrations of radioactive isotopes decrease rapidly at depths $\gtrsim$20 km, even small concentrations in a mass 300 times as great as that of the lithosphere could powerfully affect antineutrino production. And while the total quantities of U and Th could not exceed twice those in the lithosphere without violating the constraints imposed by the total heat flux, K and Rb concentrations are not as constrained and, indeed, on some geophysical models, total K may be 10 times that in the lithosphere[8,12,14]. Since essentially all antineutrinos produced within the Earth reach the surface without interacting, it follows that our estimates of surface flux must be underestimates, perhaps substantial.

From Table 1, the total antineutrino flux normal to the Earth's surface due to all decays in the lithosphere is of the order of 10^7 cm^{-2} s^{-1} in an energy range up to 3.26 MeV, four orders of magnitude less than the solar neutrino flux of 10^{11} cm^{-2} s^{-1} for low-energy (<1 MeV) neutrinos. Above ~1 MeV, the spectral

† Permanent address: Lyman Laboratory of Physics, Harvard University, Cambridge, Massachusetts 02138, USA.

Table 1 Chief radioactive isotopes in the lithosphere ($m = 2\times10^{25}$ g)

Isotope	$t_{1/2}\times1.44$ (s)	% Isotope abundance	Element abundance by weight	Flux $\bar{\nu}$ ($cm^{-2}\,s$)	Integrated flux	E_{max} (MeV)	Heat generation ($cal\,g^{-1}\,s^{-1}$)	Total heat (W)
^{40}K	5.7×10^{16}	0.01	2.6×10^{-2}	3×10^{6}	1.1×10^{7}	1.31	7.2×10^{-13}	1.8×10^{12}
^{87}Rb	2.1×10^{18}	28	3.1×10^{-4}	1.3×10^{6}	4.6×10^{6}	0.274	1.8×10^{-13}	0.2×10^{12}
^{232}Th*	6.3×10^{17}	100	1.9×10^{-5}	$2.4\times10^{5}\times4=9.6\times10^{5}$	3.5×10^{6}	2.25	6.3×10^{-9}	7.3×10^{12}
^{238}U*	2×10^{17}	99	4×10^{-6}	$2.4\times10^{5}\times6=9.6\times10^{5}$	3.5×10^{6}	3.26	2.4×10^{-8}	9.6×10^{12}
			Total	6×10^{6}	2×10^{7}			19×10^{12}

* Data include decay chain.

region in which the terrestrial antineutrino intensity is greatest (see below), the solar flux is of the order of $\sim10^{8}\ cm^{-2}\,s^{-1}$. Thus in this region of the spectrum, we may expect the terrestrial signal to be perhaps one order of magnitude and not four weaker than that due to solar neutrinos. Geometry further enhances the terrestrial signal, as will be seen, if the source distribution is a shell near the surface.

The quantity relevant for antineutrino measurement, which we call $F_{\bar{\nu}}$, is the antineutrino flux at the surface integrated over all directions. This can be expressed as a radial integral in terms of the antineutrino production rate per unit volume $n_{\nu}(r)$, which is directly related to the distribution of radioactive sources. If R is the radius of the Earth,

$$F_{\bar{\nu}} = \frac{1}{2R}\int_0^R n_{\nu}(r)\, r \ln\frac{1+r/R}{1-r/R}\,\mathrm{d}r \qquad (2)$$

If $n_{\nu}(r)$ is constant in a shell going from the surface to some smaller radius s, equation (2) can be integrated exactly to yield:

$$F_{\nu} = \frac{3}{2}\frac{N_{\bar{\nu}}}{4\pi R^2(1-s^3/R^3)} \times\left[(1-s/R)\left[1+1/2[1+s/R]\log\left[\frac{1+s/R}{1-s/R}\right]\right]\right] \qquad (3)$$

where $N_{\bar{\nu}}$ is the total rate of antineutrino emission from the Earth. This function varies from 3.5 ($N_{\bar{\nu}}/4\pi R^2$) for a shell of depth ~30 km, to 1.5 ($N_{\bar{\nu}}/4\pi R^2$) for a uniform distribution throughout the Earth, to 1.0 ($N_{\bar{\nu}}/4\pi R^2$) for a distribution concentrated at the Earth's centre. For this last distribution, all the flux is normal to the Earth's surface and thus the integrated flux is equal to the normal flux. For all other distributions, integrated fluxes are enhanced relative to normal flux estimates. However, surface distributions (like the ones we consider here) are only enhanced by a factor ~2 compared with uniform distributions, implying that sensitivity to significant abundances deep inside the Earth is not lost. (We use a conservative estimate of 30 km as the shell size here. A smaller value could increase the base signal from the lithosphere as can be seen from equation (3).)

This is taken into account in both Table 1 and Fig. 1, which presents the total flux ($F_{\bar{\nu}}$) per unit energy of antineutrinos from the lithosphere, calculated using an appropriately normalized allowed β-decay spectrum for ^{40}K, ^{87}Rb and each of the β^- emitters in the U and Th chains. Figure 1 shows that there are several well defined peaks and plateaus in the terrestrial antineutrino spectrum related to decays of the four chief isotopes of Table 1. Figure 2 shows the expected antineutrino/neutrino spectrum at the Earth from all sources over a wide range of energies including the solar and terestrial peaks, black-body neutrinos and antineutrinos, and a background of antineutrino from supernovae.

Essentially all antineutrinos produced inside the Earth reach the surface without interaction. Thus their measurement would be an ideal probe of the Earth's interior and be useful for studying regions inaccessible by other means. With direct sampling we can probe at best the upper mantle region in contact with the lithosphere using the outflow from volcanoes. Modulo small enhancement factors for surface distributions, however, the antineutrino signal gives a whole Earth measurement. Subtracting known contributions from the lithosphere gives a direct measurement of the internal properties of the Earth. Important geophysical information which can, in principle, be obtained by measuring the antineutrino flux from different radioactive isotopes is given below.

(1) **U, Th.** Uranium and thorium decays are responsible for most of the heat production inside the Earth. The associated antineutrino flux, therefore, gives a direct measurement of heat production inside the Earth due to radioactivity. These antineutrinos are produced only in radioactive decays and are not related to any other heat source, or to residual heating. Thus we can determine that component of heat flow produced from radioactivity. This both allows a better determination of whether the Earth is cooling and provides energetic data for understanding the Earth's dynamics. Also, determination of internal abundances of U and Th imparts information on the geology of the Earth's mantle and core—in particular to check the assumption that this radioactivity is concentrated on the surface, and also in the continental crust[9].

(2) **^{40}K.** Table 1 shows that ^{40}K decays produce the largest overall flux from the lithosphere. The abundance of ^{40}K is sensitive to geology, and is assumed to be zero in dunites and in the mantle and core. However, as its abundance is not constrained by heat flow considerations, any amount of ^{40}K in the interior could increase the flux due to ^{40}K decays by perhaps a factor of 10 (ref. 14). The sensitivity of ^{40}K to rock type means that a measurement of such a large flux could provide important data on the composition of the mantle and core.

(3) **^{87}Rb.** Measurement of the low-energy antineutrinos from ^{87}Rb can have important implications for our understanding of convection currents in the upper mantle. These currents are assumed to be of the order of 700 km in depth[9] and during solidification of the crust transported Rb from the upper mantle to the crust. How much the abundance of ^{87}Rb in the crust differs from its whole Earth value thus gives an indication of how much material has been deposited in the crust, and thus of how deep this upper mantle is[9]. This convection layer is also related to the dynamics of heat storage. Determining the amount of internal heat generated by radioactivity can also shed light on how much is being stored, and hence on the size and dynamics of the outer convection layer.

Detecting low-energy antineutrinos

Antineutrinos with energies in the MeV range interact with nuclei producing radiochemical transitions from (A, Z) to $(A, Z-1)$ atoms through two different weak interaction processes related to the inverse of the β-decay process (see equation (1)):

$$(A, Z-1) \rightarrow (A,\ Z) + e^- + \bar{\nu} + Q_{\beta}$$

where Q_{β} represents the energy release beyond the rest energy

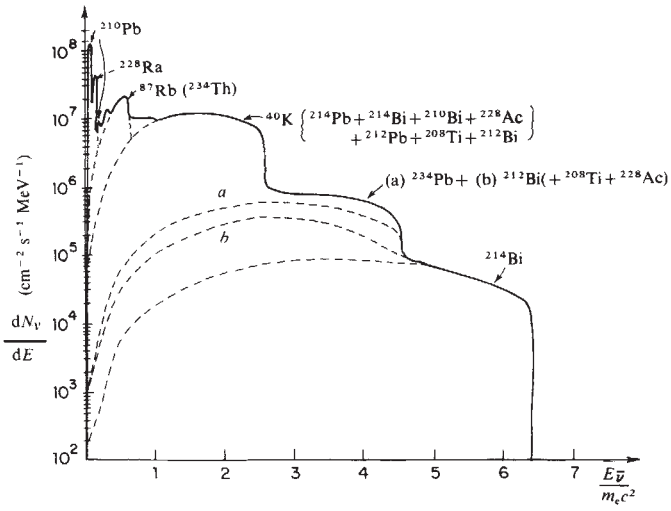

Fig. 1 Number density of antineutrinos at the Earth's surface due to abundance of chief radioactive isotopies in the lithosphere.

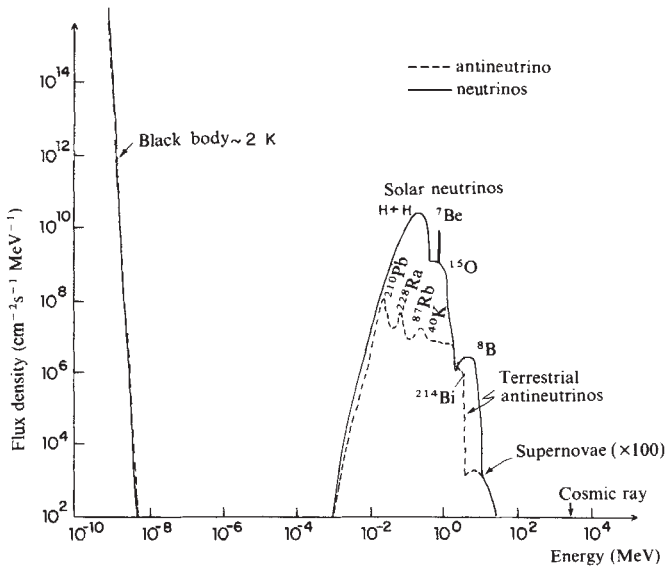

Fig. 2 Spectrum of neutrinos and antineutrinos at the Earth's surface (continuous sources in cm^{-2} s^{-1} MeV^{-1}, line sources in cm^{-2} s^{-1}. Supernovae peak is enhanced by a factor of ~100).

of the electron. By interchanging particles in the initial and final state we can consider the reactions:

$$(A, Z-1) \leftarrow (A, Z) + e^- + \bar{\nu} + Q_\beta \qquad (4a)$$

$$e^+ + (A, Z-1) \leftarrow (A, Z) + \bar{\nu} + Q_\beta + 1.02\ \text{MeV} \qquad (4b)$$

Note their differing kinematics. Process (4*a*) (resonant orbital electron capture[15]) has threshold energy identical to the related β-decay process, but occurs as a resonant process only for incoming antineutrinos in a small range around this energy. Process (4*b*) (inverse β decay), on the other hand, requires an additional 1.02 MeV of energy for the incoming antineutrino, but can occur for all energies above this threshold. Thus these processes can be exploited to probe different energy regions of the terrestrial antineutrino spectrum (Fig. 1).

In addition, each of the two processes predominates in different regions of the (A, Z) space of target atoms. The cross-section for the resonant process is given by[15]:

$$\sigma_{res} \sim S \frac{1.66 \times 10^{-40}}{(137)^3} |\psi(R_0)|^2 \frac{\rho(E_{res})}{ft}\ \text{cm}^2 \qquad (5)$$

where $|\psi(R_0)|^2$ is the probability density for the electron at the nuclear surface, ft is the 'reduced lifetime' characterizing the nuclear matrix element for the related β decay, $\rho(E_{res})$ is the density of antineutrinos per unit energy interval at the resonant energy, and S is a spin-statistics factor for the final state. As $|\psi(R_0)|^2$ increases with increasing Z, equation (5) is maximized for detectors with high Z, and low ft values (allowed transitions).

Note that the dependence of σ_{res} on $\rho(E_{res})$ implies an enhanced interaction rate for incoming antineutrino distributions which are sharply peaked in the region of the resonance. In particular, low-energy sources such as ^{87}Rb can have large $\rho(E)$ values (see Fig. 1) without extremely large integrated flux densities. To obtain Fig. 1, we used $\rho(E)$ for allowed β transitions, including the Coulomb correction factor which biases the antineutrino spectrum towards higher energies[16], and using known ft and $\tilde{Q}_B$ values for the relevant terrestrial isotopes. As terrestrial decays are not of the allowed type, the actual $\rho(E)$ would be slightly modified by factors enhancing the ends of the spectrum[17]. We approximated these effects by normalization of $\rho(E)$.

The inverse β-decay cross-section is energy dependent and is given by[16]:

$$\sigma_{\bar{\nu}}(\varepsilon) = S \frac{2.6 \times 10^{-41}}{ft} F(Z, \varepsilon')(\sqrt{\varepsilon'^2 - 1})\varepsilon' \qquad (6)$$

where $\varepsilon' = \varepsilon - Q_B - 1$ is the energy of the emitted positron (in units of the electron mass), and $F(Z, \varepsilon')$ is the Coulomb factor which tends in this case to suppress the cross-section near threshold with increasing Z. The total interaction rate is obtained by integrating equation (6) over the range of available energies, weighted by the factor $\rho(E)$.

Thus, process (4*a*) increases for higher detectors, while process (4*b*) decreases, and (4*a*) is favoured for narrow spectra, while (4*b*) is more sensitive to broader spectra going to higher energies.

These differences can be exploited in detector design to maximize sensitivity to different antineutrino sources. Low Z detectors will tend to involve inverse β-decay interactions which will be sensitive to the higher-energy terrestrial β decays of ^{40}K, ^{238}U, ^{232}Th, while high Z detectors can, through resonant capture, pick out peaks in the spectrum, such as those at low energy for ^{87}Rb and ^{212}Pb decay. We now consider two model detectors, one at high Z and one at low Z; these were chosen without regard to actual experiments. Table 2 shows the calculated interaction rates for the detectors ^{3}He and ^{209}Bi. These results justify our expectations.

Finally, before considering the practicality of antineutrino detection, we consider whether the total interaction rates of Table 2 may be increased significantly using different detectors. First, for inverse β decay we recall that detection efficiency is maximized for detectors with low Z, low ft values and low $\tilde{Q}_\beta$. ^{3}He is the lowest Z stable product of a β-decay except for a free proton, and $\tilde{Q}_\beta$ for the transition, $^{3}\text{H} \rightarrow {}^{3}_{2}\text{He}$ is even lower than the $n \rightarrow p$ transition. Also, as $\log ft \geq 3$ with equality for transitions which are both allowed and favoured, and thus have maximal nuclear wave function overlap, $^{3}_{2}$He is the optimal inverse β-decay type detector. Thus the maximal possible interaction rate due to antineutrinos from the lithosphere along which interact through inverse β decay is of the order of 0.4 TAU (SNU). Of course, this number may increase by up to an order of magnitude due to antineutrinos from the rest of the Earth.

The maximum resonant capture rate is more difficult to determine. The rate of 0.2 TAU in the ^{209}Bi model detector is about the same order as the maximum inverse β decay in the He detector. ^{209}Bi is the highest Z stable product of a β^- decay, and hence optimizes this aspect of resonant capture. However, the ft value of this detector ($\log ft = 5.5$) is over two orders of magnitude greater than that of the He detector. Since $\sigma \sim (ft)^{-1}$, a high Z target with $\log ft \sim 3$ would have a detection rate of $\sim 10^2$ TAU which is not possible.

The table of isotopes indicates that there is no ground state-to-ground state transition with $ft \sim 10^3$. We might, however, expect

Table 2 Two model detectors

Terrestrial process	E_ν max	$^3_2He \rightarrow {}^3_1H$ H_1 lifetime = 12.3 yr $\log ft = 3.1$ $Q_B = 0.01861$ MeV Rates Resonant (TAU)	Rates Inverse (TAU)	$^{209}Bi \rightarrow {}^{209}Pb$ Pb lifetime = 3.3 h $\log ft = 5.5$ $Q_B = 0.64$ Rates Resonant (TAU)	Rates Inverse (TAU)
^{40}K	1.31	1.8×10^{-9}	0.11	8.5×10^{-2}	0
^{87}Rb	0.274	3.1×10^{-7}	0	0	0
^{238}U					
^{234}Th	0.191	5.2×10^{-9}	0	0	0
^{234}Pa	2.29	2.3×10^{-9}	0.11	10^{-4}	1.2×10^{-5}
^{214}Pb	1.03	1.4×10^{-9}	0	8.5×10^{-2}	0
^{214}Bi	3.26	4×10^{-11}	5.3×10^{-2}	2.8×10^{-3}	9×10^{-6}
^{218}Pb	0.061	9×10^{-8}	0	0	0
^{210}Bi	1.16	1.2×10^{-9}	1.4×10^{-2}	1.1×10^{-2}	0
^{232}Th					
^{228}Ra	0.055	2.5×10^{-5}	0	0	0
^{278}Ac	2.18		1.4×10^{-2}	6×10^{-3}	10^{-7}
^{212}Pb	0.58	$0(10^{-9}-10^{-11})$	0	0	0
^{212}Bi	2.25		3.1×10^{-2}	10^{-5}	6×10^{-6}
^{208}Tl	1.80		2.8×10^{-2}	10^{-4}	2×10^{-6}
Total from lithosphere		2.5×10^{-5}	0.36	0.2	2.6×10^{-5}

1 TAU = 10^{-36} interactions per target atom s^{-1} (and is equivalent to 1 SNU).

that a transition from an (A, Z) nuclei to an excited state of some $(A, Z-1)$ nuclei may have much better wave function overlap producing a minimal $\log ft$ value. This is not possible because such a value occurs when the proton making the transition does not change nuclear levels. For all stable high Z nuclei, $n_{neutron} \gg n_{proton}$, and therefore all proton-to-neutron transitions must result in level changes, implying at best a $\log ft \geq 4.5$ (ref. 16).

Thus transitions to excited states cannot significantly increase resonant cross-sections compared with that of ^{209}Bi, and if $Z < 83$ for such detectors then any increase due to a slightly reduced ft value is largely compensated by the Z dependence of the cross-section. Some gains can be made if $Q_\beta < 0.274$ MeV so that the detector is sensitive to low-energy antineutrinos since $\rho(E)$ for these antineutrinos is greater by at least a factor of 2 (see Fig. 1) compared with those in the range of the ^{209}Bi detector. In general, however, for both the inverse β decay and resonant capture processes, the total interaction rate of antineutrinos due to decays in the upper lithosphere is always ≤ 0.5 TAU.

(Antineutrino interactions may also be measurable by non-radiochemical means, such as water type targets using photodetection of γ rays associated with antineutrino scattering[17]. However, these cannot distinguish the antineutrino signal from comparable or larger signals because of other background effects, and solar neutrinos.)

An interaction rate of 0.5 TAU translates into an event rate of $\sim(1\ \text{AMU}/M_{nucleus})$ events h^{-1} $kton^{-1}$ of detection material. Whether this is acceptable depends on the feasibility of amassing 1 kton of reasonable detection material, and then extracting the signal from the background. For comparison, we consider closely related solar neutrino experiments.

The Brookhaven solar neutrino experiment utilizes the reaction $\nu + {}^{37}Cl \rightarrow {}^{37}Ar + e^-$, which is the inverse of the electron capture decay of ^{37}Ar, with a half life of 35 days (ref. 1) and a threshold of 0.81 MeV. ^{37}Cl, with an isotopic abundance of 25% is easily obtainable. A 400,000-l (0.6 kton) tank of perchlorethylene, C_2Cl_4, was used as a detector and placed underground in the Homestake Gold mine at a depth of ~1,500 m to reduce cosmic-ray production of ^{37}Ar. The ^{37}Ar produced (along with a little ^{36}Ar placed in the tank to check recovery efficiency), being a noble gas is easily removed from the liquid by purging with helium gas. After its separation from the helium, its radioactive decay is measured to determine the net production of ^{37}Ar. A production rate of $\sim 2.0 \pm 0.3$ SNU (= TAU) is obtained, with a background from known sources of ~0.35 SNU (ref. 1). The actual ^{37}Ar production rate was ~1 atom per 2 days.

To detect antineutrino event rates of the order of ~1 per day the following aspects of the ^{37}Cl experiment must be reproduced.
(1) To obtain ~1 event per day due to 0.5 TAU (at best), of the order of 1 kton of material must be available. The material must be cheap to produce, or to borrow (as it is not destroyed in the detection process).
(2) Because of the extremely small number of atoms produced, separation techniques must be almost 100% efficient. This is possible for reaction products which are noble elements. If this is not the case, more sophisticated chemical separation must be possible. Also, use of a liquid or gas detector for separation purposes seems most feasible.
(3) If radiochemical detection is envisioned the reaction product must have a lifetime long enough for significant production to occur but short enough so that subsequent decays can be measured—of the order of 1 day $< \tau <$ 1 yr.

The model targets discussed demonstrate the maximum possible detection rates due to the two interaction processes. They were not selected for their practicality. Actual targets may have detection rates which are significantly less than these maximum values. Table 3*a* gives a complete list of all stable target materials with $A_Z \rightarrow A_{Z-1}$ transitions induced by antineutrinos, and with product lifetimes >1 day.

Table 3 shows that there are no allowed ground-state transitions which involve noble gas products. Indeed, the only such process, Rb → Kr, is strongly suppressed both in ground-state and excited-state transitions. This implies that the proven separation technology from the ^{37}Cl solar neutrino experiment cannot be used in antineutrino detection. Other chemical separation techniques are possible, however, especially if the chemistry of target and product differ significantly as in the case of Cl or Br, whose products can undergo reduction reactions and subsequent water layer separation (R. Davis Jr, personal communication).

Next we observe that all ground-state transition rates are at least an order of magnitude smaller than the $^3He \rightarrow {}^3H$ reaction. In particular the ^{35}Cl reaction which might be considered because it could utilize the same tank and materials as the solar neutrino experiment and has reasonable chemistry for separation, would only result in a transition rate of ~1 atom yr^{-1}. ^3He is unlikely to be available in large enough quantities and thus we must consider measuring rates of $10^{-1} - 10^{-2}$ TAU, or else utilizing transitions to excited states. As the $Zn \rightarrow {}^{64}Ni$ reaction which seems to be the next favoured ground-state transition

Table 3 Antineutrino targets with product lifetime ≥1 day and $Q_{ns} < 2$ MeV (in order of increasing log ft)

Target process	Q_B (MeV) (ground state transition)	log ft	Product lifetime	Interaction rate (TAU)	Sensitivity to terrestrial decay
$^{3}_{2}He \rightarrow {}^{3}_{1}H$	0.0186	3.1	12 yr	0.32	^{238}U, ^{40}K, ^{232}Th
$^{33}_{16}S \rightarrow {}^{33}_{15}P$	0.248	5.0	25 day	0.002	^{232}Th, ^{238}U, ^{87}Rb
$^{35}_{17}Cl \rightarrow {}^{35}_{16}S$	0.167	5.0	88 day	0.004	^{232}Th, ^{238}U, ^{87}Rb
$^{121}_{51}Sb \rightarrow {}^{121}_{50}Sn$	0.383	5.0	27 h	0.01	^{40}K, ^{238}U
$^{64}_{30}Zn \rightarrow {}^{64}_{29}Cu \rightarrow {}^{64}_{28}N_i$	0.573	5.3	Stable	0.02	^{40}K, ^{238}U, ^{232}Th
$^{77}_{34}Se \rightarrow {}^{77}_{33}As$	0.68	5.7	1.6 day		
$^{175}_{71}Lu \rightarrow {}^{175}_{70}Vb$	0.467	6.3	5.5 day	$\sim 10^{-2}$	
$^{169}_{69}Tm \rightarrow {}^{169}Er$	0.34	6.4	9.4 day		
$^{185}_{75}Re \rightarrow {}^{185}_{74}W$	0.49	6.5	75 day		
$^{177}_{72}Hf \rightarrow {}^{177}_{71}Lu$	0.497	6.6	6.7 day		
$^{63}_{29}Cu \rightarrow {}^{63}_{28}Ni$	0.067	6.7	92 yr	0.04* (0.15–0.2 MeV)	^{87}Rb, ^{232}Th
$^{153}_{63}Eu \rightarrow {}^{153}_{62}Sm$	0.801	7.2	2 day		
$^{199}_{80}Hg \rightarrow {}^{199}_{79}Au$	0.46	7.5	3.15 day		
$^{151}_{63}Eu \rightarrow {}^{151}_{62}Sm$	0.076	7.6	87 yr	0.15 (0.15–0.23 MeV)	^{87}Rb, ^{232}Th
$^{141}_{59}Pr \rightarrow {}^{141}_{58}Ce$	0.58	7.7	33 day		
$^{161}_{66}Dy \rightarrow {}^{161}_{65}Tb$	0.58	7.8	7 day		
$^{155}_{64}Gd \rightarrow {}^{155}_{63}Eu$	0.248	8.2	1.8 yr		
$^{14}_{7}N \rightarrow {}^{14}_{6}C$	0.156	9.0	5×10^3 yr		
$^{85}_{37}Rb \rightarrow {}^{85}_{36}Kr$	0.67	9.1	10.7 yr		
$^{113}_{49}In \rightarrow {}^{113}_{48}Cd$	0.58	9.2	14 yr		
$^{39}_{19}K \rightarrow {}^{39}_{18}Ar$	0.565	9.9	269 yr		
$^{204}_{82}Pb \rightarrow {}^{204}_{81}Tl$	0.765	9.9	3.8 yr		
$^{79}_{35}Br \rightarrow {}^{79}_{34}Se$	0.154	10.8	6.5×10^4 yr	0.08 (0.25 MeV)	^{87}Rb, ^{232}Th
$^{107}_{47}Ag \rightarrow {}^{107}_{46}Pd$	0.035	10.8	7×10^6 yr		

Estimate excited state transition interaction assuming log $ft = 5.0$ for allowed transition. Excited state Q_B given in parentheses.

after He would result in an event rate of only ~1 atom per month per kton, the second possibility seems appropriate unless detectors larger by at least an order of magnitude than the ^{37}Cl detector are envisioned.

Rates for transitions from ground state to excited state, if they are allowed, can, for high Z atoms, approach or equal the ^{209}Bi rate of ~0.2 SNU. This can lead to event rates of the order of 1 per day. However, because the radioactive lifetime of many of product atoms (once they have relaxed to their ground state) is too long to use radiochemical detectors we must consider new technology for separation of the product atoms and for their subsequent detection. However, new methods, such as resonant ion spectroscopy, make detection of small number of 'stable' atoms possible. Current sensitivity for resonant ion counting is about 100–1,000 atoms. Such values can, in principle, be produced with running times of the order of a year. Note that proposals exist for proton decay detectors which will measure stable decay product atoms[18]. A proton lifetime of $\sim 10^{31}$ yr corresponds to a rate of $\sim 3 \times 10^{-3}$ TAU. For long-lived transition products, the possibility of archeological detection might be considered by searching for products which can have accumulated over long periods in ordinary rock. However, such abundances would be at best of the order of $\sim 10^{-19}$.

The experimental situation with regard to terrestrial antineutrino detection today is similar to that at the time when the first experiments for solar neutrinos were designed. Large-scale machines using new technology will be required, probably exploiting excited state transitions (possibly ^{79}Br) with rates at best ~0.1–0.2 TAU and new resonant ion spectroscopy techniques.

Other aspects of the experimental situation are encouraging. First, such detectors will be able to be calibrated using nuclear reactor antineutrinos: this was not possible for solar neutrino detectors. Such calibration is important both for terrestrial antineutrino measurement and for checking cross-sections of low-energy antineutrinos on complex nuclei which have never been directly measured.

Second, terrestrial antineutrino fluxes have a known baseline—that due to known levels of radioactivity in the lithosphere—whereas ^{37}Cl solar neutrino fluxes depend on processes and abundances in the Sun which are not well known, and for which a lower limit is not easy to establish. If neutrino oscillations[19] occur (with three neutrino species) over length scales that are small compared with the radioactive shell depth, the lithospheric signal could be reduced by a factor of 3 below the expected baseline level. While many effects can increase the detection rate, if sensitivities allow an observation of such a possible reduction, this would point to neutrino oscillations.

Even a null result can be significant if the detector sensitivity were of the order of the expected lithosphere flux. As stated earlier, abundances of ^{40}K and ^{87}Rb can be significantly above those present in the lithosphere—by up to a factor of 10. Such abundances can be ruled out by null results, allowing empirical tests of some geophysical models. Finally, as excited state detectors have long-lived final products, longer running periods and hence increased sensitivity are possible.

Whether such first generation terrestrial antineutrino detectors would yield more information than similar solar neutrino detectors depends on the possible backgrounds. These we separate into four types: nonantineutrino-induced events, antineutrinos from other terrestrial sources and from local radioactive deposits, and extraterrestrial antineutrino backgrounds. The extraterrestrial background is discussed below.

Unless the background for the terrestrial antineutrino experiment is less than that of the known background in the ^{37}Cl solar neutrino experiment (~0.3 SNU) it will overwhelm the signal. The background for both experiments originates from cosmic ray muons. In the case of solar neutrino detectors, secondary protons can mimic ν induced reactions through a (p, n) type replacement. For antineutrino detection, however, it is either tertiary neutrons (from spellation reactions), or stopped muons themselves which can mimic the terrestrial antineutrino signal—in the first case by (n, p) type interactions, or in the second through an inverse β-decay type process involving muon capture.

We believe the second background is more problematic than the first. Deep underground, average surviving muon energies will be of the order of ~300 GeV (ref. 20). Most spellation neutrons created in the detector will not lose sufficient energy in the detector volume to result in $A_Z \rightarrow A_{Z-1}$(n, p) reactions

which do not further disrupt target atoms. Also, slow neutrons from the surrounding rock outside the detector (from local radioactivity as well as spellation effects) can be absorbed if suitable shields are placed around the detector. Thus we concentrate our quantitative analysis on the case of stopped muons.

At the depth of the Brookhaven Cl detector[17], muons are stopped at an average rate of 2×10^{-3} ton^{-1} day^{-1}. Whether these are captured and mimic antineutrino-induced transitions depends both on the capture probability and the probability that no neutrons are emitted from the excited nucleus after muon capture[21]. The first probability increases strongly with Z, while the second is generally small (<10%) (see ref. 21). Also, using the fact that the stopping rate is a function of density, we find that for high Z targets the muon background at these depths should be about equal to the antineutrino signal for excited-state detectors with detection rates of ~0.2 TAU. For low Z targets it is $\ll$0.2 TAU. However, the only efficient detector at low Z is the ^{3}He. Thus we consider three possible ways to reduce this background. First, at only slightly greater depths the stopped muon rate drops asymptotically to ~1/10 their value at the Davis experiment depth[17]. Then, one might dope the detector with high Z efficient muon capturing material to reduce to number captured by desirable target atoms. A combination of these techniques may reduce this background to 10–20% of the antineutrino signal. One could determine quantitatively both this background, and that due to neutrons by using radiochemical detectors with Q_β values $\gtrsim$2 MeV which are insensitive to terrestrial antineutrinos but will react with neutrons and stopped muons.

Antineutrinos from other terrestrial sources consist primarily of atmospheric antineutrinos from cosmic-ray muon and pions, but we have also considered possible backgrounds from sources such as proton decay and nuclear weapons testing. Extrapolating fluxes of atmospheric neutrinos and antineutrinos estimated by other authors[22–24], to low energies, we estimate a maximum flux density of the order of 10^{-3} cm^{-2} s^{-1} MeV^{-1} in the 1–10 MeV range. This background, even if it were to remain constant up to 50–100 MeV, would give $\ll$1% effect, both for resonant capture type detectors sensitive only to low-energy antineutrinos, and for inverse β-decay detectors which are also sensitive up to higher energies. With regard to possible antineutrino backgrounds from proton decay, with a proton lifetime of $>10^{31}$ yr (ref. 25), even if the dominant decay mode is to antineutrinos the maximum flux is of the order of 10^{-4} cm^{-2} s^{-1} and is again negligible. Nuclear weapons explosions, on the other hand, can yield pulses of antineutrinos from the decay of fission products. However, a 1 Mton explosion at 1,000 miles from the detector will yield a maximum pulse of 10^{10} antineutrinos which, while momentarily swamping the terrestrial flux, yields a signal which is equivalent to that obtained in only 1 h of running time in the constant flux due to radioactivity. Thus unless the detector is built very close to a test site this background is also negligible. (Similar results apply for backgrounds from reactors.)

In discussing signal enhancement from local radioactivity, we assume that radioactive distributions are uniform in a shell ~30 km in depth from the surface, with an average concentration so that total abundances in the lithosphere agree with known values. Except for an enhancement factor (~3.5), the flux through the surface can be written

$$F_{\bar{\nu}} = \frac{C_{a\nu}V_{\text{shell}}}{4\pi R_e^2} = \frac{C_{a\nu}\frac{4}{3}\pi[R_e^3-(R_e-d)^3]}{4\pi R_e^2} \quad (7)$$

where $C_{a\nu}$ is the average lithosphere source concentration, V the volume of the surface shell, d = 30 km (depth of shell). Now since $d \ll R$ we can expand equation (7) to obtain in first order:

$$F_{\bar{\nu}} = C_{a\nu}d \quad (8)$$

Hence the relevant scale in the problem is the shell thickness d.

Thus, modulo geometric factors, we need only consider the quantity $F_{\bar{\nu}}' \approx C_{\text{local}}d_{\text{local}}$, where C_{local} is the enhanced concentration of a local source of scale size d_{local}, to see if local sources can overwhelm the global signal.

Whether these conditions are satisfied depends on the actual distribution of radioactive ore. For example, the minimal allowable $C_{\text{ore}}/C_{a\nu}$ for uranium to be minable is ~10^3 (refs 26, 27). But the largest single deposit in the United States, Jackpile, contains an ore body some 1,300 ft wide, 2,000 ft long, 20 ft in average thickness, ranging from surface outcroppings to a depth of 2,000 ft (ref. 27). Even assuming an optimal surface layer, we get $F_{\bar{\nu}_{\text{local}}} = 5\,F_{\bar{\nu}_{\text{lithosphere}}}$ for a detector directly above the distribution, which is too small a signal (of the order of 1 TAU) to make such prospecting practical.

Larger-scale enhancement of radioactive abundances may be of more geological interest, however. Indeed, the continental crust is expected to have an enhanced concentration of radioactive isotopes compared with the lithospheres as a whole[13]. Such enhancement could increase the measured signal compared with our estimates based on a spherically symmetric distribution. (Also, for constant total radioactivity, a smaller shell depth than we assumed could increase the signal compared with our initial estimates.) In general, however, as far as initial global measurements are concerned, while large-scale local region >0(30 km) of enhanced deposits exist[28], only the major deposits, which can easily be avoided, might yield signals significantly greater than the mean global signal.

However, regions exist where it is expected that radioactive abundances may be significantly less than average. For example, heat flow under the oceans has been modelled as being due to convective plate formation, rather than radioactivity[13]. Some empirical confirmation of this large-scale anisotropy might be possible if detectors with sensitivity below the expected lithospheric level were placed in the ocean.

Thus, the only background which may pose difficulty for extracting the large-scale terrestrial antineutrino signal is that due to cosmic-ray muons, and we believe this can be reduced to an acceptable level in a way which can be checked independently.

Extraterrestrial antineutrinos

Except for rare nearby supernovae pulses, the solar neutrino flux masks all other possible extraterrestrial sources in the 0.1–15 MeV range. The terrestrial antineutrino flux is both smaller and more localized in energy, and will we believe, make antineutrino rather than neutrino detectors more useful for astrophysical purposes. In particular, a diffuse background of antineutrinos (and neutrinos) from supernovae exists which, if detectable, can yield information on supernova frequency in galaxies. First, however, we consider other astrophysical sources which do not produce antineutrino fluxes comparable with the terrestrial flux.

Antineutrinos are absent from all major solar reactions. This is important because even if their production rate was suppressed by 10^{-4}–10^{-5} relative to solar neutrinos, their flux on Earth could equal that of terrestrial antineutrinos.

In describing this suppression, we note that all 18 reactions in the p–p cycle, and the CNO cycle involve the production of neutrinos or photons only[28]; thus antineutrino production is divorced from the primary energy production mechanisms of the Sun, and we must consider other weak interaction processes involving neutrino pair production[28], however, these are strongly suppressed, and are not significant until temperatures of order ~10^9 K (ref. 28). At solar temperatures they are down by factors of the order of $\lesssim10^{-10}$. Because of its distance from Earth, in order for fluxes due to β^- decays in the Sun to compete with fluxes for terrestrial β^- decay, radioactive isotopic abundances on the Sun must be greater by a factor of ~10^6. No solar model predicts such abundances.

Having demonstrated that essentially no solar antineutrino flux exists, we may consider other point sources. As the terrestrial antineutrino flux is of the order of 10^{-4} times the solar neutrino flux, the antineutrino luminosity of any source must be of the

order of $L \sim 10^{-4}\,(L_{sun})(R/R_{sun})^2$ to compete with the terrestrial antineutrino flux. This rules out all known continuous point sources as significant sources of antineutrinos. Even the flux of neutrino and antineutrinos from the galactic centre is, for energies of interest, expected to be orders of magnitude smaller than the atmospheric neutrino flux which is much smaller than the terrestrial flux[22].

Only supernovae explosions, which emit $\sim 10^{53}$ erg of energy, mostly in the form of neutrinos and antineutrinos with energies ~ 10 MeV (ref. 29), are, in principle, energetic enough to produce fluxes comparable or larger than the solar or terrestrial fluxes. However, calculations using existing supernovae neutrino detectors demonstrate that a 1 kton detector will only be sensitive to supernovae in our Galaxy[29]. These explosions are expected to occur at a rate of only 1 every 10–30 yr, making individual detection problematic.

If supernovae have been occurring at a constant rate of 1 per 15 yr per galaxy for most of the history of the Universe (say $\sim 10^{10}$ yr), their cumulative effects would have produced a diffuse background of neutrinos and antineutrinos. The neutrino background is hidden by the high-energy portion of the solar neutrino flux. However, the antineutrino background is, in principle, separable from the terrestrial flux.

We can calculate the present antineutrino luminosity at the Earth, taking into account the effects of Universe expansion as follows[30]. Each particle emitted with energy E at cosmic time t_i will be redshifted at observation time to the energy $ER(t_i)/R(t_0)$, where $R(t)$ represents the cosmic scale factor describing isotropic homogeneous expansion. Similarly, antineutrinos emitted at intervals δt_i will arrive at time intervals $\delta t_i R(t_0)/R(t_i)$. Hence the apparent luminosity (energy/unit area/time) of a supernova at co-moving coordinate r_i (relative to the Earth) is

$$l = \frac{LR^2(t_i)}{4\pi R^4(t_0) r_i^2} \tag{9}$$

where L is the absolute luminosity of the supernovae in antineutrinos.

Now the number of supernovae observed at t_0, which occurred between time $t_i - \delta t_i$ and t_i, is:

$$dN = n(t_i) 4\pi R^2(t_i) r_i^2 \delta t_i \tag{10}$$

where n is the number density of supernovae per unit time.

Thus the total energy density of neutrinos and antineutrinos is measured by an observer on Earth at time t_0 is:

$$\rho_{\nu,\bar{\nu}} = \int_{t_s}^{t_0} n(t_i) L \left[\frac{R(t_i)}{R(t_0)}\right]^4 dt_i \tag{11}$$

where t_s is the initial time of supernovae occurrence, which can be taken to zero without affecting the numerical result. If supernova frequency has been constant, so that $n(t_i) = n(t_0)[R(t_0)/R(t_i)]^3$, equation (11) can be integrated to yield:

$$\rho_{\nu,\bar{\nu}} = \eta(t_0) L \int_0^{t_0} \frac{R(t)}{R(t_0)}\, dt = \frac{3}{5}\eta(t_0) L t_0 \tag{12}$$

Thus the net effect of expansion is to reduce the neutrino energy density by a factor 3/5 compared with what could be expected in the absence of expansion. Now assuming $\sim 10^{53}$ erg emitted per supernova, and that $\eta(t_0) \sim 10^{-3}$ Mpc^{-3} yr^{-1} (this is only a rough estimate, the actual densities of galaxies may be less. The frequency we assume may also be too low[31]), equation (12) gives

$$\rho_{\nu,\bar{\nu}} = 3 \times 10^{-14} \text{ erg cm}^{-3} = 2 \times 10^{-8} \text{ MeV cm}^{-3} \tag{13}$$

The mean energy per antineutrino (neutrino) is ~ 10 MeV at the time of emission is now redshifted by the same factor of 3/5 of equation (12). Hence, the total flux density of neutrinos and antineutrinos through a small volume at the Earth's surface is now

$$N(\nu, \bar{\nu}) = \frac{\rho_\nu^c}{6} \sim 10^2 \text{ cm}^{-2} \text{ s}^{-1} \tag{14}$$

If roughly half the energy is emitted in the form of antineutrinos[29] then the number density of antineutrinos at the Earth's surface at present is ~ 50 cm^{-2} s, with a spectrum peaked at ~ 6 MeV. This number could increase if the frequency of supernovae increased at earlier times.

This flux is not large enough to warrant an experiment for its determination. However, antineutrino detectors may eventually be sensitive to these antineutrinos. As their mean energy is significantly larger than terrestrial antineutrinos, they may yield an effect at the $\sim 1\%$ level for inverse β-decay type detectors. If this small effect could be measured, it would yield the first estimate of the time-averaged supernovae frequency per galaxy over the lifetime of the Universe.

Conclusions

The neutrino and antineutrino fluxes described here are shown on Fig. 2. Neutrinos provide information on the Sun and stellar processes, and antineutrinos provide information on the Earth, and perhaps on supernova abundance. Both processes provide information which is probably inaccessible by means other than weak interaction probes. The absence of electromagnetic interactions for neutrinos and antineutrinos implies that they may open for investigation an orthogonal and complementary component of the Universe to that available through electromagnetic detection. Moreover, neutrinos and antineutrinos may account for much of the energy density of the Universe, and hence may have a vital role in its dynamics.

Yet the aspects of the weak interactions that make them so useful for investigating the interior of the Sun and Earth also hinder their measurement. Detection of terrestrial antineutrinos will require sophisticated new technology. We can envision several generations of experiments aimed at measuring different parts of the antineutrino spectrum. If this proves possible, we may obtain the first fundamental empirical data on the Earth's interior structure and dynamics, including measurements of heat production, convection in the upper mantle, geological data on interior composition and perhaps information on local concentrations of, or global anisotropies in radioactive abundances. Also, it may be possible to gain information on the abundance and frequency of supernovae, on the antineutrino component of cosmic rays on possible neutrino oscillations, and to verify theoretical predictions of low-energy weak interaction cross-sections.

It is a long step from even a single meassurement to the programme outlined above. Indeed, even rudimentary weak interaction astronomy and geophysics may not become practicable for some time. In principal however, neutrino and antineutrino astronomy and geophysics can open vast new windows for exploration above us and below.

We thank our colleagues, including M. Turner, S. Bludman, F. Wilczek, E. Fireman, R. Clayton, K. Lande, R. Davis, A. Yahil, R. Wagoner, E. Purcell and N. Isgur, for useful discussions. In particular, M. Turner corrected an error in initial flux calculations and R. Davis informed us on experimental matters and of past work on this subject. L.M.K. and D.S. also thank the Aspen Institute of Physics where this work was initiated. Finally, we thank W. Hampel for criticism which improved the paper in many ways—in particular by pointing out the backgrounds due to stopped muons.

1. Bahcall, J. N. *Rev. mod. Phys.* **50**, 881–903 (1978).
2. Davis, R. Jr, Evans, J. C. & Cleveland, B. T. in *Conf. Proc. Neutrinos-78* (ed. Fowler, E. C.) (Purdue University Press, 1978).
3. Eders, G. *Nucl. Phys.* **78**, 657–662 (1966).
4. Marx, G. *Czech. J. Phys.* **B19**, 1471–1479 (1969).
5. Marx, G. & Lux, I. *Acta phys. acad. sci. hung.* **28**, 63–70 (1970).
6. Avilez, C., Marx, G. & Fuentes, B. *Phys. Rev.* **D23**, 1116–1117 (1981).
7. *Conf. Proc. Cosmological and Geological Implications of Isotope Ratio Variations* (National Academy of Sciences Publ. 572, 1958).
8. Jeffreys, H. *The Earth* 5th edn (Cambridge University Press, 1970).
9. Mackenzie, D. P. *Scient. Am.* **249**, 67–78 (1983).
10. Sclater, J. G., Parsons, B. & Jaupart, C. *J. geophys. Res.* **86**, 535–552 (1981).
11. *Handbook of Chemistry & Physics* (Chemical Rubber Co., Florida, 1982).
12. Jaupart, G., Sclater, J. G. & Simmons, G. *Earth planet. Sci. Lett.* **52**, 328–344 (1981).

13. Sclater, S. G., Jaupart, C. & Galson, D. *Rev. Geophys. Space Sci.* **18**, 269–311 (1980).
14. Lubimova, E. B. in *Earth's Crust and Upper Mantle* (ed. Hart, P. J.) (Washington, DC, 1969).
15. Mikaelyan, L. A., Tsinoev, B. G. & Bereyai, A. A. *Soviet J. nucl. Phys.* **6**, 254–256 (1968).
16. Segre, E. *Nuclei and Particles* (Benjamin, Reading).
17. Particle Data Group *Phys. Lett.* **111B** (1982).
18. Fireman, E. L. in *Proc. int. Cosmic Ray Conf.* Kyoto, Vol. 13 (1979).
19. Frampton, P., Glashow, S. L. & Yildiz, A. (eds) *First Workshop on Grand Unification* (Mathematical Science Press, Brookline, 1980).
20. Cherry, M. L. *et al. J. Phys. G., nucl. Phys.* **8**, 879–885 (1982).
21. Charalambus, S. *Nucl. Phys.* **A166**, 145–161 (1971).
22. Margolis, S. H., Schramm, D. N. & Silverberg, R. *Astrophys. J.* **221**, 990–1002 (1978).
23. Stecker, F. W. *Astrophys. J.* **228**, 919–927 (1979).
24. Gaisser, T. K., Stanev, T., Bludman, S. & Lee, H. Preprint (Bartol Research Inst., 1983).
25. Bionta, R. M. *et al. Phys. Rev. Lett.* **51**, 27–30 (1983).
26. Laney, C. A. *Metallic and Industrial Mineral Deposits* (McGraw-Hill, New York, 1966).
27. Skinner, B. J. *Earth Resources* (Prentice-Hall, New Jersey, 1976).
28. Reeves, H. in *Stars and Stellar Systems* (eds Aller, L. H. & Mclaughlin, D. P.) (University of Chicago Press, 1965).
29. Bethe, H. A., Yahil, A. & Brown, G. E. *Astrophys. J. Lett.* **262**, L7–L10 (1982).
30. Weinberg, S. *Gravitation and Cosmology* (Wiley, New York, 1972).
31. Tammann, G. in *Supernovae* (ed. Schramm, D. N.) (Reidel, Dordrecht, 1977).

ARTICLES

Origin of diamonds in old enriched mantle

S. H. Richardson*, J. J. Gurney†, A. J. Erlank† & J. W. Harris‡

* Center for Geoalchemy, Department of Earth, Atmospheric and Planetary Sciences, Massachusetts Institute of Technology, Cambridge, Massachusetts 02139, USA
† Department of Geochemistry, University of Cape Town, Rondebosch 7700, South Africa
‡ Department of Applied Geology, University of Strathclyde, Glasgow G1 1XJ, UK

Sub-calcic garnets encapsulated by diamonds from relatively young (90 Myr) kimberlites in southern Africa, yield ancient Sm–Nd and Rb–Sr model ages (3,200–3,300 Myr). The chemistry and distribution of these and associated sub-calcic garnets from kimberlite concentrate, indicate diamonds formed following enrichment of residual sub-cratonic mantle such as that remaining after widespread extraction of 3,500-Myr komatiitic lavas.

ALTHOUGH diamonds have been recovered directly from kimberlite pipes for more than a century, their relation to host kimberlite has remained controversial[1–3]. The debate centres on whether diamonds are phenocrysts or xenocrysts in the proto-kimberlite magma. More broadly, diamond crystallization may be temporally and spatially associated with kimberlite genesis, or, alternatively, segments of mantle within the diamond stability field may be littered with diamonds, so that sampling by kimberlite is strictly accidental. Diamond is, in fact, only a trace constituent of kimberlite, with abundances varying from zero to an order-of-magnitude maximum of 1 p.p.m. Moreover, in southern Africa, kimberlites erupted within the boundaries of the Archaean craton are diamondiferous, while those in adjacent younger mobile belts are barren[4].

A small fraction of diamonds (<1%) contains syngenetic monomineralic and rarely multimineralic inclusions belonging to peridotitic or eclogitic parageneses. The peridotitic inclusion assemblage, which includes olivine, orthopyroxene, chromite and distinctive lilac chrome-pyrope garnet, is on average far more abundant than the eclogitic assemblage of orange pyrope-almandine garnet and omphacitic clinopyroxene[5–7]. This categorization and relative abundance are apparently also reflected in diamond carbon isotope compositions[8], most of which have been recorded in inclusion-free diamonds[9]. Thus, constraints on diamond origin derived from such inclusions may be considered applicable to most inclusion-free diamonds.

Diamond inclusion assemblages parallel the mineralogy of the two most important categories of mantle xenolith in kimberlites, garnet peridotite and eclogite. However, there are significant differences in chemical composition between the dominant peridotitic diamond inclusions and constituent minerals of garnet peridotites. For example, garnets in diamond have significantly higher Mg and Cr, and lower Ca, contents than their peridotite xenolith counterparts, which are generally saturated with Ca (Fig. 1). The former are here referred to as sub-calcic garnets. Lilac garnets of similar but less extreme composition have also been found in kimberlite concentrate[10]. The distribution of these discrete sub-calcic garnets in southern African kimberlites generally mirrors that of diamonds, implying an intimate genetic association[11].

Previous radiogenic isotope studies on trace constituents of diamond-related materials have been viewed with some scepticism, given identification and potentially severe contamination problems. For example, a U–Pb study of presumed sulphide inclusions in diamonds yielded model Pb ages in excess of 2,000 Myr but was clouded by uncertainty regarding inclusion identity and paragenesis[12]. Similarly, results of a He isotopic study of industrial-grade diamonds required speculation on He entrapment by diamonds soon after accretion of the Earth[13].

We have investigated the Sm–Nd and Rb–Sr isotopic systematics of carefully screened sub-calcic garnets in concentrate and diamonds from two of the best documented localities in southern Africa, Kimberley (28°46′ S, 24°48′ E) and Finsch (28°16′ S, 23°06′ E; ~160 km WNW of Kimberley). These kimberlites are respectively representative of two classic types of kimberlite (basaltic and micaceous) recognized on the basis of petrographic, chemical and isotopic characteristics[14,15]. Our consistent results preclude a genetic connection between diamonds and host kimberlites and provide strong age and chemical constraints on an ultimate origin of diamonds in old, enriched mantle.

Sub-calcic garnets in diamonds

Garnet inclusions in diamond are easily recognized *in situ* by their distinctive colours. Peridotitic inclusions, of which 10–20% are garnets, comprise more than 98% of inclusions in Finsch diamonds[7] and more than 90% of those in Kimberley diamonds[16]. A comprehensive study of inclusion major element compositions[17], revealed that more than 95% of peridotitic garnets in Finsch diamonds have extremely high Mg and Cr and low Ca contents. Associated olivine and orthopyroxene inclusion compositions are also extremely magnesian with average values of Mg/(Mg+Fe) of 0.941 and 0.949 respectively[17]. Peridotitic diopside inclusions are conspicuous by their absence, emphasizing the residual major element character of the peridotitic inclusion paragenesis[5–7].

Lilac garnet, inclusion bearing, diamonds were selected from the −6+5 and −7+6 diamond sieve fractions[18] of the general production from Finsch and the Kimberley Pool. The latter represents output from Bultfontein, De Beers, Dutoitspan and Wesselton, the four kimberlite pipes currently mined at Kimberley, which are close enough at surface to have possibly had the

* Present address: Institut de Physique du Globe, Université de Paris VI, 4 Place Jussieu, 75230 Paris Cedex 05, France.